Journal of Template

Vol. 00, No. 0, 0000

Efficient Global Optimization Applied to Design and Knowledge Discovery of Supersonic Wing *

Masahiro Kanazaki**, and Naoto Seto**

**TokyoMetropolitanUniversity,

6-6 Asahigaoka, Hino-shi, Tokyo 191-0065, Japan

E-mail: kana@sd.tmu.ac.jp

Abstract

Efficient global optimization (EGO) was applied to the multi-objective design and knowledge discovery of a supersonic transport (SST) wing. The objective functions considered here are employed to maximize the lift–to-drag ratio at supersonic cruise, to minimize the sonic boom intensity and to minimize wing structural weight, simultaneously. The EGO process is based on Kriging surrogate models, which were constructed using several sample designs. Subsequently, the solution space could be explored through the maximization of expected improvement (EI) values that corresponded to the objective function of each Kriging model because the surrogate models provide an estimate of the uncertainty at the predicted point. Once a number of solutions have been obtained for the EI maximization problem by means of a multi-objective genetic algorithm (MOGA), the sample designs could be used to improve the models' accuracy and identify the optimum solutions at the same time. In this paper, 108 sample points are evaluated for the constructions of the Kriging models. In order to obtain further information about the design space, two knowledge discovery techniques are applied once the sampling process is completed. First, through functional analysis of variance (ANOVA), quantitative information is gathered and then, self-organizing maps (SOMs) are created to qualitatively evaluate the aircraft design. The proposed design process provides valuable information for the efficient design of an SST wing.

Keywords: Supersonic Wing, Multidisciplinary Design, Efficient Global Optimization, Analysis of Variance, Self-organizing Map

1. Introduction

Recently, several techniques have been proposed for the efficient design of real-world aircrafts based on numerical simulations. In Ref [(1)], a multi-fidelity approach was adopted for the design of a supersonic transport (SST) wing. Specifically, two regression models were constructed in order to evaluate its aerodynamic performance. The first model was based on a low-fidelity/ low-cost full potential solver, and the second was based on a high-fidelity/high-cost Euler solver. The next step was to evaluate the differences between the two models. On the basis of the differences, additional design samples were selected and evaluated using the high-fidelity solver in order to enhance the global model. In Ref [(3)], efficient global optimization (EGO), i.e., optimization based on Kriging surrogate models was applied to solve real-world design problems with less computational cost. EGO proved to be effective for global search when combined with heuristic methods, like the genetic algorithm (GA)[(4)]. Thus, the EGO process could identify the global optimum with a relatively low evaluation cost. Obayashi, et al. proposed the multi-objective design exploration (MODE) [(5)]; a set of non-dominated solutions were obtained using EGO for the multi-disciplinary design optimization (MDO) of a transonic wing using EGO, and the

*Received XX Xxx, 200X (No. XX-XXXX)
[DOI: 00.0000/ABCDE.2006.000000]

design knowledge was discovered by means of data mining techniques such as self-organizing maps (SOMs)[6] and rough set theory[7]. In authors' previous study [8], EGO was also applied to solve the design problem of a high-lift airfoil and acquire useful information.

As stated above, an efficient design is required to solve real-world problems. Therefore, the surrogate model based design exploration can be potentially employed for the multi-disciplinary design and knowledge discovery of a SST wing with airframe configuration such as the supersonic business jet (SSBJ)[9]. In this study, EGO is applied to the wing design of the silent SST demonstrator (S^3TD)[10]-[11], as shown in Fig. 1(a), which is developed by Japan Aerospace Exploration Agency (JAXA). The design problems of a supersonic aircraft includes many requirements such as lower drag, lower structural weight, lower noise at take-off/landing, and lower sonic boom at supersonic cruise. In other words, the design problems are multifaceted. In addition, the complex geometry of the aircraft consisting of the main wings, fuselage, and horizontal/vertical tail wing need to be taken into consideration. Conventionally, aircraft's wing design has been considered that the lift by the wing equal to the aircraft weight. In such design, trim balance by the horizontal tail should be considered after the wing is designed, and the drag by the horizontal tail is not always minimized. As this result, there is possibility of increasing the total drag, even if the drag of the main wing has been minimized. With these facts, this study proposes the design methodology which consider not only the lift constraint but also the trim constraint, simultaneously; 'the lift equal to the weight' and 'the momentum around the gravity center is zero by the setting of the horizontal tail.' In such design condition, the number of the evaluation becomes higher. This disadvantage can be resolved by the employment of EGO process, and the design exploration can be satisfyingly carried out in practical time.

The design problem on which the focus in this study is the design optimization of supersonic wings that can help achieve a relatively high lift-to-drag ratio (L/D), low sonic boom intensity (ΔP) defined in Fig. 1(b), and low structural wing weight (W_{wing}). Namely, the design problem addressed in this study is MDO, and has three objectives: first, to maximize the L/D, second, to minimize the ΔP, and lastly, to minimize the W_{wing}. During the EGO process, several sample designs are obtained using design of experiment (DOE) [2][4]. The aerodynamic performance of the obtained sample designs is evaluated by means of computer-aided design (CAD)-based automatic panel analysis (CAPAS) developed at JAXA [10]-[11] in consideration of two aerodynamic constraints about the lift and the moment of the aircraft. With the use of CAPAS, the pressure distribution along the aircraft surface can be obtained and the L/D can be calculated. CAPAS can also estimate the ΔP on the ground. W_{wing} is estimated by exploiting MSC.NASTRAN™.

During the EGO process, non-dominated solutions of the multi-objective design problem are explored efficiently by means of the DOE and the Kriging-based multi-objective genetic algorithm MOGA. After selecting design samples, Kriging-based functional analysis of variance (ANOVA) [2][5][8][12] and SOMs[4][8] are used to extract useful design knowledge. ANOVA, a multivariate analysis method is used to acquire quantitative information about the contribution of each design variable to the objective functions. Through these analyses, information necessary to solve fundamental design problems can be obtained. The next step is to put SOMs to practical use. This is a "data mining" method widely used to project multidimensional data onto a two-dimensional (2D) map. Through this visualization, qualitative information useful to solve design problems can be obtained.

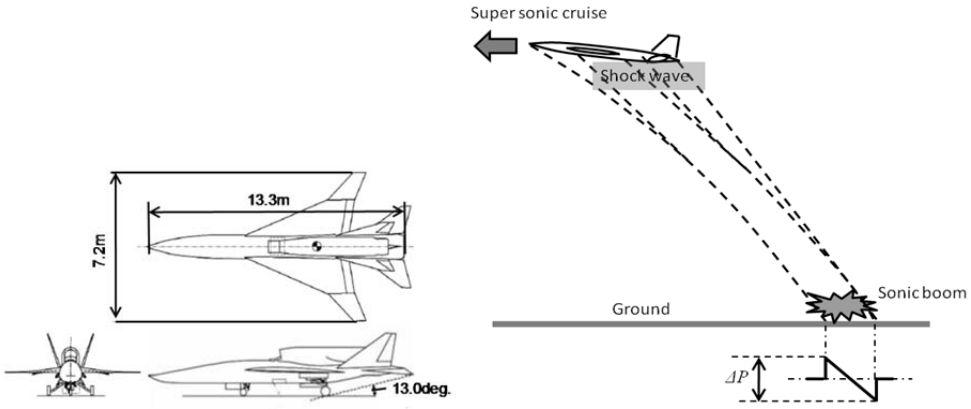

(a) (b)

Fig. 1 S^3TD designed by JAXA: (a) Conceptual design [10], and (b) Definition of sonic boom intensity.

2. The EGO Procedure

The optimization procedure followed for the design of the S^3TDconsists of the following steps (see Fig. 2). First, N design samples are selected by means of Latin hypercube sampling (LHS)[2][5][8][13] which is a space filling method and then assessed for the construction of a Kriging surrogate model. Second, n additional design samples are added and the design's accuracy is improved by constructing a new Kriging model based on all $N+n$ samples. It should be noted that the n additional samples are selected using expected improvement (EI) maximization[2][4][5][8][14]. Furthermore, MOGA is applied to solve this maximization problem. This process is iterated until the improvement of the objective functions becomes negligible. Finally, the non-dominated front is examined, while data mining techniques are applied to obtain the further information about the design problem. Each step of the optimization procedure is described in detail in the following sections.

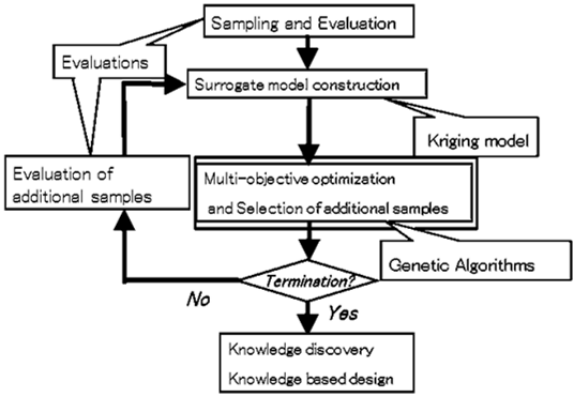

Fig. 2 Procedure for the efficient exploration of the global design model

2.1. Kriging surrogate model

The Kriging model express the value $y(x^i)$ at the unknown design point x^i as

$$y(x^i) = \mu + \varepsilon(x^i) \quad (i = 1, 2, \ldots, m), \tag{1}$$

where m is the number of design variables, μ is a mean value of the objective function among all samples and $\varepsilon(x^i)$ represents a local deviation from the global model. The correlation between $\varepsilon(x^i)$ and $\varepsilon(x^j)$ is strongly related to the distance between the corresponding points, x^i and x^j. In the Kriging models, the local deviation at an unknown point x is expressed using stochastic processes. Specifically, a number of design points are calculated as sample points and then interpolated using a Gaussian random function as the correlation function to estimate the trend through the stochastic process[3].

2.2. Selection of Additional Design Samples

Once the models are constructed, the optimum point can be examined with the use of an arbitrary optimizer on the Kriging surrogate models. However, it is difficult to accurately identify the global optimum, because the Kriging surrogate models include uncertainty at the predicted point. Therefore, for the purpose of this study, EI values have been introduced as a selection criterion. The EI values for maximization problem are calculated as

$$EI(x) = (\hat{y} - f_{\max})\Phi\left(\frac{\hat{y} - f_{\max}}{s}\right) + s\phi\left(\frac{\hat{y} - f_{\max}}{s}\right) \tag{2}$$

and the EI values for the minimization problem as:

$$EI(x) = (f_{\min} - \hat{y})\Phi\left(\frac{f_{\min} - \hat{y}}{s}\right) + s\phi\left(\frac{f_{\min} - \hat{y}}{s}\right) \tag{3}$$

where f_{max} and f_{min} are the maximum and minimum value among all the available sample points and $\hat{y}$ the value calculated by Eq. (1) at an unknown point x. On the other hand, Φ and ϕ are the standard distribution and normal density, respectively. Lastly, the EI values are estimated based on the predicted function value and its uncertainty. Consequently, the solution that corresponds to a relatively large function value and large uncertainty may be the solution sought. In other words, by selecting the point where $EI(x)$ takes the maximum value as an additional sample point, the robust exploration of the global optimum and the improvement of the model can be simultaneously achieved, as shown in Fig. 3(a), because this point has a relatively large probability to be the global optimum.

In this study, a multi-objective problem is considered. Thus, to decide select additional samples, the EI values corresponding to each different objective function should be simultaneously maximized. In this study, a divided range MOGA (DRMOGA) [8][15] was employed to obtain non-dominated solutions by solving these multi-objective problems. To improve each Kriging model, several non-dominated solutions can be used as to select additional sample designs. Here, the k-means clustering method [16] is applied to cluster the non-dominated solutions, and the sample designs that are the closer to the centroid of each cluster are selected as additional samples (Fig. 3(b)). In this study, 20 clusters were defined.

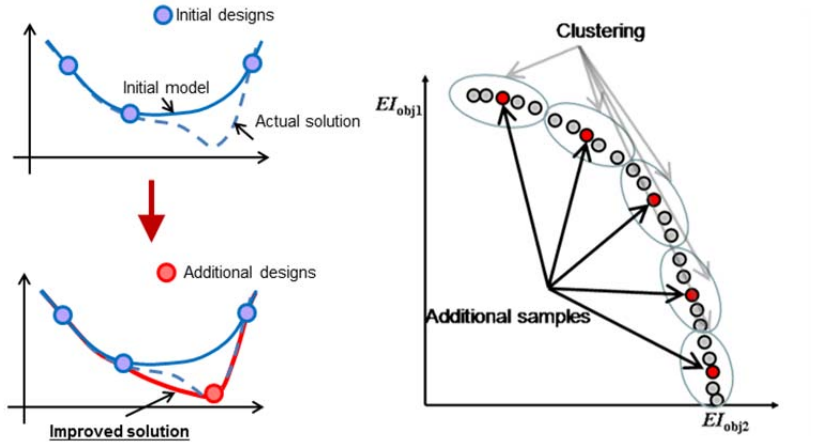

(a) (b)

Fig. 3 (a) Improvement of the global model, (b) k-means clustering and selection of additional samples based on the non-dominated solutions derived through EI maximization.

2.3. Knowledge Discovery Techniques

2.3.1. ANOVA

ANOVA, a method for multivariate analyses, is carried out to differentiate the contribution of different design variables to the variance of the responses from the global model. Specifically, to evaluate the contribution of each design variable, the total variance of the model is decomposed into the variance attributed to each design variable and the interactions between each other. The decomposition is accomplished by integrating variables out of the model $\hat{y}$. The variance of design variable x_i to μ is defined as

$$\mu_i(x_i) \equiv \int \cdots \int \hat{y}(x_1,.....,x_n)dx_1,...,dx_{i-1},dx_{i+1},..,dx_n - \mu \quad (4)$$

where the total mean μ is calculated as

$$\mu \equiv \int \cdots \int \hat{y}(x_1,.....,x_n)dx_1,.....,dx_n \quad (5)$$

The proportion of the variance attributed to the design variable x_i to the total variance of the model can be expressed as:

$$p \equiv \frac{\int [\mu_i(x_i)]^2 dx}{\int \cdots \int [\hat{y}(x_1,.....,x_n) - \mu]^2 dx_1 \ldots dx_n} \quad (6)$$

The value obtained by Eq. (6) indicates the sensitivity of an objective function to the variance of a design variable, x_i.

2.3.2. SOM

SOM are constructed by means of an unsupervised learning, nonlinear projection algorithm from a high to a low-dimensional space. This projection is based on the self-organization of a low-dimensional array of neurons. The lattice of the grid can be either hexagonal or rectangular. In this paper, the former is selected because it results in a SOM from which useful information can be easily retrieved by visual inspection.

Each neuron k on the map is represented by an n-dimensional prototype vector $\boldsymbol{m}_k = (m_{k1}, m_{k2}, \ldots, m_{kn})$ as shown in Fig. 4(a), where n is the dimension of the input vector (design space)—that is to say the number of design variables and objective functions. In the learning process, the input vector $\boldsymbol{X}$ representing a design sample is first selected and then, the nearest neuron $\boldsymbol{m}_c$ (the best matching unit, BMU) is identified using the prototype vectors of the map. The prototype vectors of the $\boldsymbol{m}_c$ and its neighbors on the grid $\boldsymbol{m}_k$ are shifted towards $\boldsymbol{X}$ as follows:

$$\boldsymbol{m}_k = \boldsymbol{m}_k + \alpha(t)(\boldsymbol{X} - \boldsymbol{m}_k) \quad (7)$$

where $\alpha(t)$ is the learning rate, and it decreases monotonically with time. This process is iterated until $\alpha(t)$ is converged enough.

During the iterative training process, the prototype vectors are also converged. The closer two patterns are in the high-dimensional space, the closer is the response of the corresponding neighboring neurons in the low-dimensional map. Consequently, SOM reduces the dimensions of the input data while preserving their features. The refined SOM is not only systematically converted into visual information, but qualitative information can also be obtained.

In this study, the commercial software modeFrontier® is used for the visualization of multidimensional data. modeFrontier® creates a map in a 2D hexagonal grid, which can be colored based on the every attribute values (for the design variables, and the objective functions). Therefore, the n component planes are visualized and can be compared easily. In the trained map, each hexagonal grid has similar vector to its neither. By coloring the grids by component values of the vector, the relationship among objective functions and design variables such as a ‘trade-off’ can be observed at a glance as shown in Fig. 4(b). However,

if the number of component planes is relatively large, they should be arranged for a comparison. Specifically, component plane reorganization can be combined with traditional correlation analysis [17]. Correlations between component pairs are revealed by the patterns observed in identical positions of the component planes, the so-called 'SOM's SOM.' Pattern matching is also possible by visual inspection. The extraction of useful design knowledge can be further simplified if all component planes are reorganized so that the most strongly correlated planes are presented next to each other.

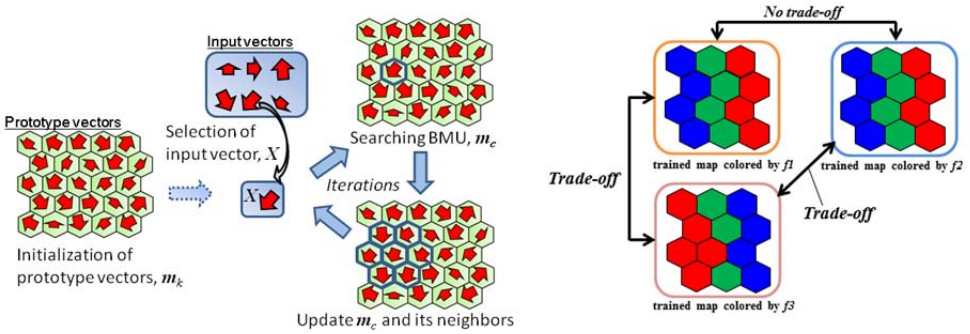

(a) (b)

Fig. 4 Self-organizing map, (a)Schematic illustration of SOM training, (b) Application example of SOM visualization example for minimization problem which has three objective functions, *f1-f3*.

3. Formulation

3. 1. Design Variables

Figure 5 shows the illustration of the supersonic wing geometry to be designed. These include the airfoil geometries (thickness and camber) of three cross sections, the sweepback angles, the twist angles, and the aspect ratio. The design variables and their range are summarized in Table1.

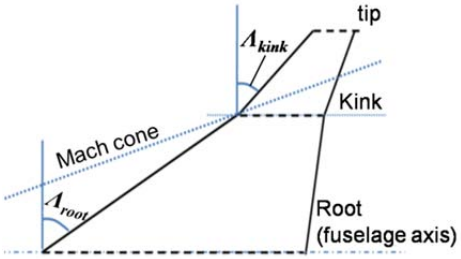

Fig. 5 Illustration of wing geometry to be evaluated

Table 1 Design variables and their values

	Design variable	Upper bound	Lower bound
*dv*1	Sweepback angle at inboard section	57 (°)	69 (°)
*dv*2	Sweepback angle at outboard section	40 (°)	50 (°)
*dv*3	Twist angle at wing root	0 (°)	2(°)
*dv*4	Twist angle at wing kink	–1 (°)	0 (°)
*dv*5	Twist angle at wing tip	–2 (°)	–1 (°)
*dv*6	Maximum thickness at wing root	3%*c*	5%*c*
*dv*7	Maximum thickness at wing kink	3%*c*	5%*c*
*dv*8	Maximum thickness at wing tip	3%*c*	5%*c*
*dv*9	Aspect ratio	2	3
*dv*10	Wing root camber at 25%*c*	–1%*c*	2%*c*
*dv*11	Wing root camber at 75%*c*	–2%*c*	1%*c*
*dv*12	Wing kink camber at 25%*c*	–1%*c*	2%*c*
*dv*13	Wing kink camber at 75%*c*	–2%*c*	1%*c*
*dv*14	Wing tip camber at 25%*c*	–2%*c*	2%*c*

3. 2. Objective Functions

The objective functions are derived through the simultaneous maximization of L/D at a target C_L, the minimization of ΔP, and the minimization of W_{wing} at supersonic cruise conditions (Mach number: 1.6). The aerodynamic performance is evaluated by means of CAPAS, as shown in Fig. 6. CAPAS includes the CATIA® v4/v5 application programming interface (API) and a full potential solver combined with a panel method [10]. The L/D and C_L are directly estimated from the pressure distribution along the aircraft surface, which can be derived with the use of the full potential solver. To evaluate the ΔP from the pressure distribution near the aircraft, Thomas's waveform parameter method [10] is used after the shockwave form has been estimated based on the pressure distribution, which is calculated around the aircraft using the Whitham's theory [10]. In this study, the speed of sound and the air density was set equal to those at an altitude of 14km.

It should also be noted that, in this study, the same structural model for wing weight estimation as Ref. [6] is employed. The inboard wing is made from aluminum, while the outboard wing is made from composite material. In addition, the inboard wing is composed of multiple frames, from the rib to the spar. The outboard wing has a full-depth honeycomb sandwich structure. In this design system, the optimization of the thickness of each frame within the inboard wing and the wing stacking sequences of the laminated composite material of the outboard wing was performed to meet concurrently the minimum weight constraints and the strength and flutter requirements. The strength characteristics were evaluated using the commercial software MSC.NASTRAN™. The conditions to which the computations corresponded were those of a symmetric maneuver at +6G, while the safety margin was set at 1.25.

To obtain the additional sample designs described in §2.2, three EI values are simultaneously maximized by means of DRMOGA. On the other hand, the EI values are calculated based on three different Kriging models; $EI_{L/D}$, $EI_{\Delta P}$ and EI_{Wwing}. Eqs. (2) and (3) are written for the present design problem as

$$\begin{cases} \textit{Maximizing} & EI_{L/D} = (\hat{y} - L/D_{\max})\Phi\left(\dfrac{\hat{y} - L/D_{\max}}{s}\right) + s\phi\left(\dfrac{\hat{y} - L/D_{\max}}{s}\right) \\ \textit{Minimizing} & EI_{\Delta P} = (\Delta P_{\min} - \hat{y})\Phi\left(\dfrac{\Delta P_{\min} - \hat{y}}{s}\right) + s\phi\left(\dfrac{\Delta P_{\min} - \hat{y}}{s}\right) \\ \textit{Minimizing} & EI_{W_{wing}} = (W_{w\min} - \hat{y})\Phi\left(\dfrac{W_{w\min} - \hat{y}}{s}\right) + s\phi\left(\dfrac{W_{w\min} - \hat{y}}{s}\right) \end{cases} \quad (8)$$

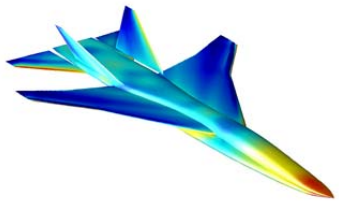

Fig. 6 Pressure distribution along the aircraft surface estimated by means of CAPAS

3. 3. Constraints

In the design problem, two aerodynamic and two geometric constraints are considered:

aero1.Target C_L=0.105 to lift the aircraft under supersonic cruise conditions

aero2.Maintain the trim balance by varying the angle of the horizontal tail wing (stabilizer)

geo1. Wing area S=21m^2

geo2. Place the kink airfoil along the fuselage axis so that the Mach cone is crossed at the leading edge of kink airfoil

The aerodynamic constraints are illustrated in Fig. 7. Because C_D is proportional to C_L^2, the pressure distribution around an aircraft is determined from three different angles of attack under cruise conditions in order to satisfy *aero1*. In addition, to meet *aero2*, the reflection angle of the stabilizer is adjusted for every aerodynamic evaluation individually. Since the pitching moment around the gravity center of the aircraft is proportional to the reflection angle, to identify the most suitable angle, each aerodynamic evaluation is conducted for two different reflection angles. Once the angle of attack and the angle of the horizontal tail are determined, the aerodynamic evaluation is conducted again under the flight conditions determined. Specifically the evaluations are conducted for each point in Fig. 7(a) to decide the reflection angle, as shown in Fig. 7(b). In total, 12 aerodynamic evaluations are required for each design sample.

Two geometric constraints are also considered. The wing area is set to 21m^2 (*geo1*) and *geo2*, about the Mach cone and main wing interaction is illustrated in Fig. 5. In the case of the S^{3}TD, the inboard wing should have a subsonic leading edge in order to achieve the high aerodynamic performance at supersonic cruise conditions. The outboard wing has a supersonic leading edge to maintain the high subsonic aerodynamic performance during landing and take-off. Therefore, the location of wing/fuselage intersection is determined for aircraft design under study according to *geo2*.

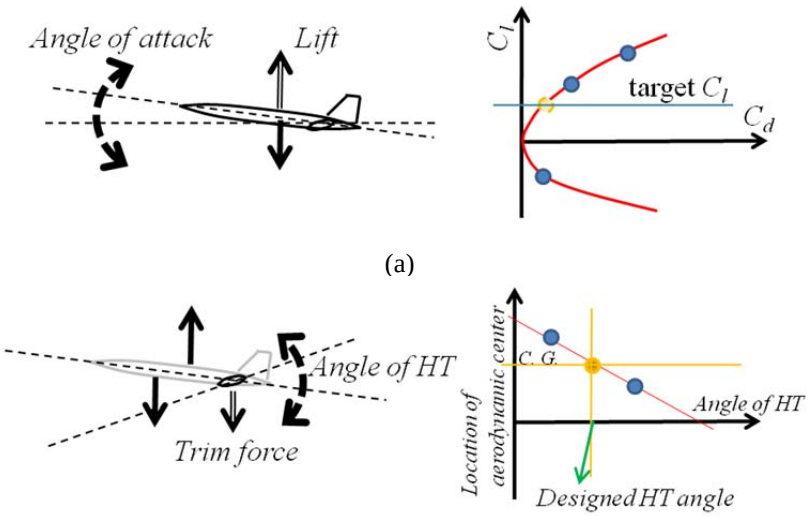

Fig. 7 Image of the geometric constraints considered in the aircraft design under study: (a)Constraint for the aircraft's lift, and (b)Constraint for the angle of the horizontal tail wing.

4. Results and Discussions

4. 1 Sampling Results

The results of the EGO process are shown in Fig. 8. Many additional samples could be added around the direction of the multi-objective optimum (non-dominated solutions, or approximate Pareto optimal set), and the trade-off between the objective functions. To compare the most promising samples for each objective function, three samples named DesA, B, and C are evaluated.

Figure9(a) shows the comparison of the geometry and pressure distribution over the surface of the 2.5th aircraft design (reference geometry defined by JAXA[7]). In the case of DesA, the highest L/D was achieved, DesB was characterized by the lowest ΔP, and DesC by the lowest W_{wing}. The value of the corresponding objective functions are summarized in

Table 2, and design variables of obtained designs are summarized in Table 3. According to Fig. 9, the outboard wing of DesA reduces the wave drag with gradual pressure variation compared with the 2.5th aircraft design. In other words, the total drag reaches a minimum, while the highest *L*/*D* is achieved. DesB is characterized by a relatively high sweep-back angle at the inboard wing and consequently, lower shock wave. Namely, the sonic boom intensity on the ground should be reduced. Lastly, in the case of DesC, the lowest W_{wing} was achieved because this aircraft design is characterized by a relatively low sweep-back angle. Due to the low sweep–back angle, the shockwave produced by the aircraft at supersonic speed is more intense and *ΔP* the highest. An additional characteristic of the DesC is that the stabilizer increases the aircraft's lift in order to reduce the aerodynamic force developed on the main wing at supersonic cruise conditions. Therefore, the structural weight of the mail wing becomes lower. The same conclusion is drawn when the trim balance constraint (*aero2*) is considered during the aircraft design process.

Figure9(b) shows the comparison of equivalent areas [18, 19] among DesA-C. From this figure, equivalent areas of DesA, B smoothly increased. On the other hand, the equivalent area of DesC rapidly increased due to its low sweep angle of the main wing. According to the *area-rule* [18], the airframe which has the smooth variation of the equivalent area achieves low drag. In actual fact, DesA, and B achieve lower drag. Additionally, the equivalent area of DesB is increased gentler than that of DesA around the main wing (about 10m). This result agreed with *Darden's sonic boom minimization theory* [19]. These results suggest that the CAPAS evaluation was in good qualitative agreement with low drag/low boom theories.

From Fig. 9(a), DesC has the smallest sweep back and the smallest aspect ratio among DesA-C, and 2.5th design. According to the theory of wing structure [18], the W_{wing} should be lighter if the wing is designed smaller sweep back and aspect ratio.

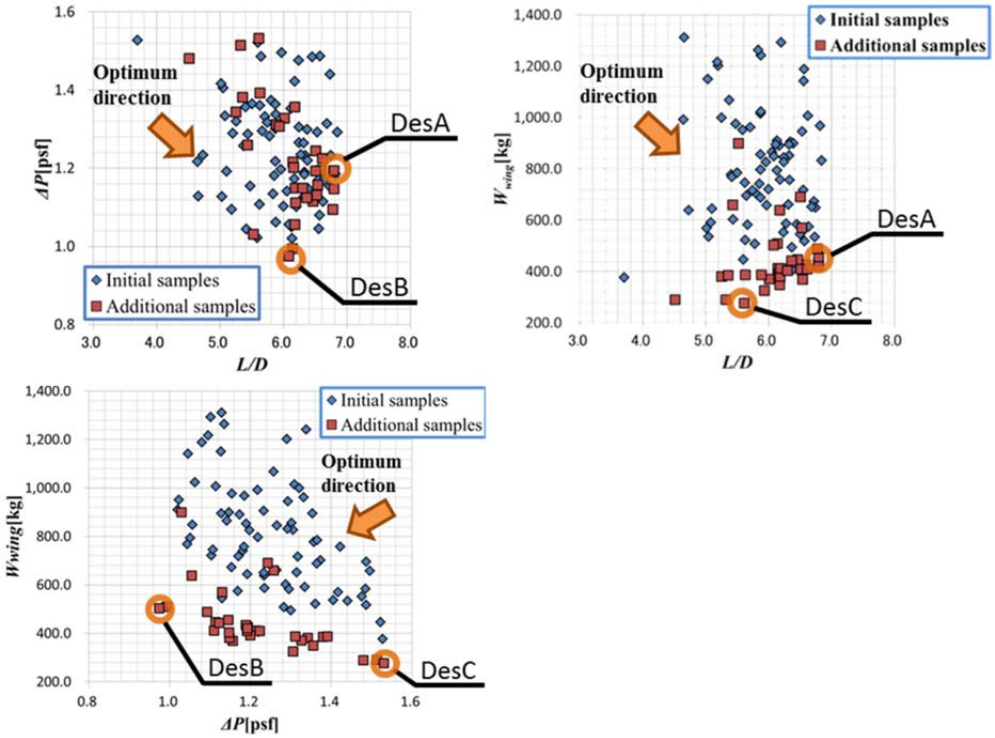

Fig. 8 Solutions obtained by means of EGO

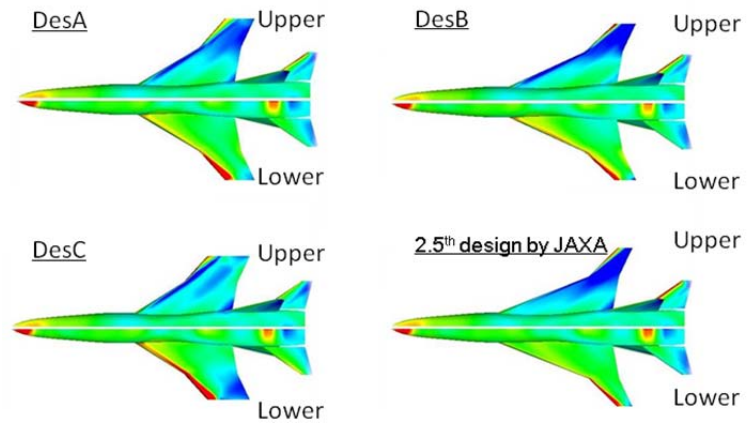

(a)

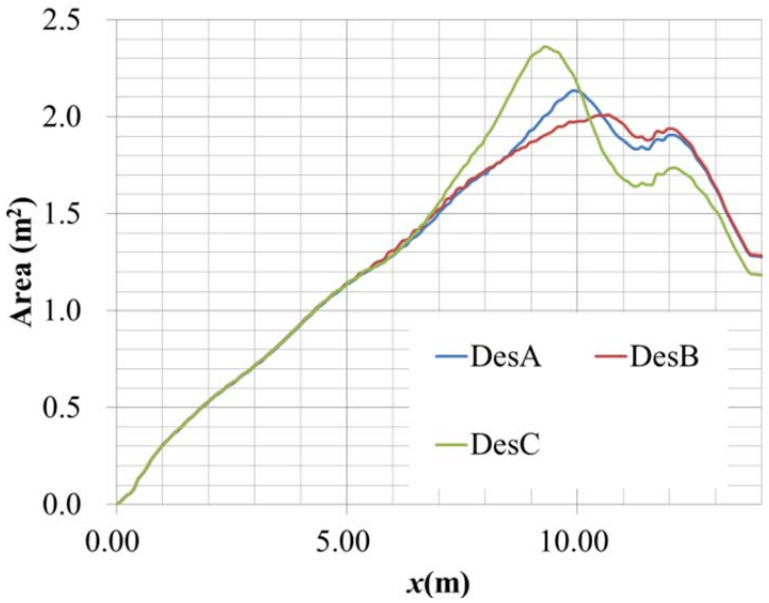

(b)

Fig. 9 Solutions picked up from EGO sampling, (a)Comparisons of geometry and pressure distribution between selected designs and reference design (2.5th design provided by JAXA), (b)Comparison of equivalent area distribution

Table 2Comparison of aerodynamic/structural performance of selected aircraft designs and reference design

	L/D	*ΔP*	W_{Wing}
DesA	7.2	1.09	806
DesB	6.7	0.96	993
DesC	5.6	1.53	276
2.5th design by JAXA	6.9	0.97	691

Table 3 Comparison of design parameters among selected designs

	Design variable	DesA	DesB	DesC
*dv*1	Sweepback angle at inboard section	58.84	64.98	57.33
*dv*2	Sweepback angle at outboard section	41.11	46.32	41.71
*dv*3	Twist angle at wing root	1.27	1.80	1.30
*dv*4	Twist angle at wing kink	-0.93	-0.98	-0.79
*dv*5	Twist angle at wing tip	-1.43	-1.20	-1.95
*dv*6	Maximum thickness at wing root	3.02	3.01	4.03
*dv*7	Maximum thickness at wing kink	3.37	3.00	4.78
*dv*8	Maximum thickness at wing tip	3.23	4.95	3.16
*dv*9	Aspect ratio	2.55	2.38	2.01
*dv*10	Wing root camber at 25%*c*	-0.47	-0.21	0.01
*dv*11	Wing root camber at 75%*c*	0.18	-0.81	0.98
*dv*12	Wing kink camber at 25%*c*	0.47	0.79	-0.98
*dv*13	Wing kink camber at 75%*c*	0.73	0.89	-0.45
*dv*14	Wing tip camber at 25%*c*	-0.63	1.25	-0.35

4. 2 Design Knowledge Extracted by ANOVA

Figure 10 shows the main effects and the two-way interaction of the design variables for each objective functions considered in this design problem. According to Fig. 10(a), *dv10-13*, which defines the inboard wing cambers, has a predominant influence on *L*/*D*, suggesting that the inboard wing design is important under supersonic cruise conditions because the inboard wing has subsonic leading edge meeting the geometric constraint *geo2*.

According to the Fig. 10(b), *dv1*, which is the sweep-back angle of the inboard wing, has a significant influence on *ΔP*. This result suggests that *ΔP* can be remarkably reduced when the most appropriate design of the inboard wing has been identified. The same conclusion can be drawn from Fig. 9.

According to the Fig. 10(c), *dv9*, *dv12*, and *dv13* influence W_{wing}. Specifically, *dv9* defines the aspect ratio. In theory, aspect ratio has a non-negligible influence on the wing structural weight. On the other hand, *dv12* and *dv13* determine the kink camber that has a non-negligible influence on the aerodynamic force acting on the wing. The aerodynamic force acting on the wing needs to be also considered during the wing structure design. Because the kink airfoil influences the geometry of both the inboard and outboard wing, this result suggests that the kink camber should be carefully designed in order to achieve the lowest possible wing weight.

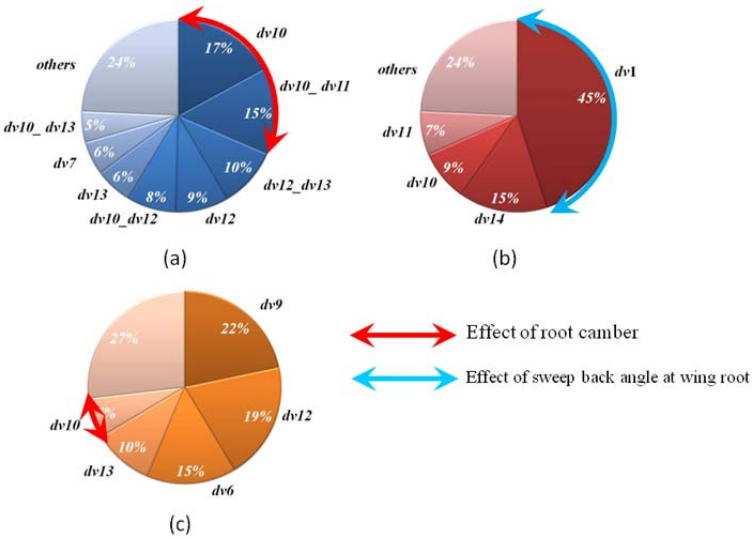

Fig. 10 ANOVA results showing effect of design variables on objective functions: (a)*L*/*D*, (b)Δ*P*, and (c)W_{wing}.

4. 3 Design Knowledge Extracted by SOM

To generate SOM, the objective functions are used as training data, and the trained map is colored according to the objective functions, the reflection angle of the stabilizer, and design variables. Namely, colored component planes for 18 attribute values are created. These component planes are arranged according to their color contours and in particular, the correlation among component planes, as shown in Fig. 11. Based on this map, the correlation between different attribute values can be evaluated.

Figure 12 shows the component planes about objective functions, and the reflection angle of the stabilizer. According to this figure, the trade-off between *L*/*D* and *ΔP* is not so sever. The reason is that the aircraft fuselage geometry is same as that of the 2.5th aircraft design, and during its design, the low-boom/low-drag trade-off was taken into consideration [(7)]. On the other hand, the trade-off between *ΔP* and W_{wing} is severe, but a compromised solution can also be founded.

Further useful information about this design problem can be extracted based on the correlation shown in Fig. 11. Specifically, *L*/*D* is strongly correlated with design variables, *dv2*, *8*, and *13*. In particular, *dv2*, which is the sweep-back angle of the outboard wing, should relatively large and *dv8* relatively low in order to achieve an increase in *L*/*D* with the reduction of wave drag at the outboard wing. In addition, *dv13* has influences on *L*/*D*, because *dv13* defines kink camber as well as the geometry of the inboard wing and outboard wing. These findings are in agreement with information extracted by means of ANOVA. On the other hand, these correlations reveal the dependence of *ΔP* on the sweep-back angle of the inboard wing (*dv1*), which is in agreement with the ANOVA results.

The W_{wing} is not correlated with any other attribute values. However, comparing component planes about W_{wing} with the reflection angle of the stabilizer, an aircraft design characterize by a positive reflection angle of the stabilizer would achieve relatively low W_{wing}. In other words, while the reflection angle of the horizontal tail is generally positive to maintain the trim balance, this aircraft's lift could be achieved through not only the main wing but also the horizontal tail. This finding is in agreement with Fig. 9.

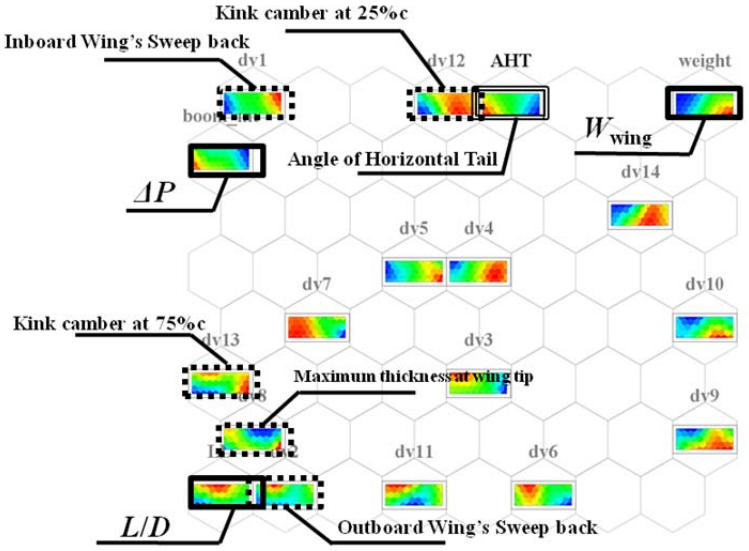

Fig. 11 Summary of SOM result self-organized according to similarity among attribute values. (Dash line: objective functions, and dotted line: design variables)

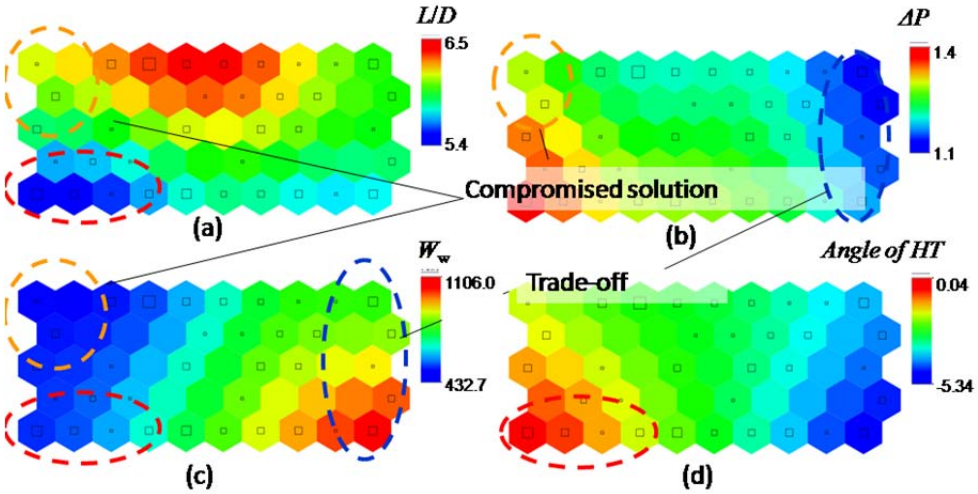

Fig. 12 Component maps colored by objective functions and angle of horizontal tail wing; (a)*L*/*D*, (b)Δ*P*, (c)W_{wing}, and (d)angle of stabilizer.

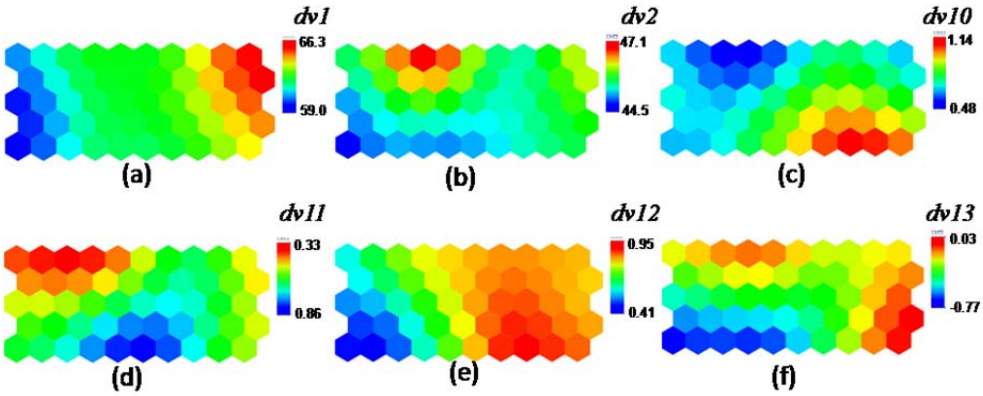

Fig. 13 Component maps colored by selected design variables; (a)*dv1*, (b)*dv2*, (c)*dv10*, (d)*dv11*, (e)*dv12*, and (f)*dv13*.

4. Conclusions

In this paper, the acquirement of the design knowledge for a silent SST, is discussed. The design objectives are the maximization of *L*/*D*, minimization of *ΔP*, and minimization of W_{wing}. The total of 105 sample designs is evaluated and their results are used for design

space analysis by proposed EGO procedure. In this process, GA is used along with Kriging surrogate models. To obtain non-dominated solutions, additional samples are selected by GA exploration based on EI values on the Kriging model. In addition, ANOVA and SOM are employed to acquire the information about the design problem. In this study, the main wing of S^3TD conducted by JAXA was designed.

Many additional samples become non-dominated solutions. According to this sampling result, trade-off among objective functions was observed. To investigate the detail of the design space, ANOVA and SOM are applied. According to these result, useful design knowledge can be acquired. According to ANOVA result, the inboard wing camber has a predominant influence on L/D. Additionally, SOM result suggest that larger outboard sweep back and thinner tip airfoil provide higher L/D wing, because outboard wing has supersonic leading edge. ΔP is influenced by the sweep back of the inboard wing. The design which achieves lowest W_{wing} has low taper ratio. Additionally, to reduce the aerodynamic force on the main wing, the reflection angle of the horizontal tail becomes positive where the horizontal tail wing also gains the lift. This knowledge could be obtained by the consideration of the trim balance constraint. Because it takes large computational cost to design the wing under such constraint, proposed design technique was highly efficient.

Acknowledgements

We wish to thank Aviation Program Group in Japan Aerospace Exploration Agency for providing us with the geometric data of the S3TD. We especially would like to thank Dr. Yoshikazu Makino and Dr. Ken Takatoya for their kind advice for our research.

References

(1) Choi, S, Alonso, J., J., and Kroo, I., M., Multi-Fidelity Design Optimization Studies for Supersonic Jets Using Surrogate Management Frame Method, *Journal of Aircraft*, Vol. 45, No.1 (2008), pp. 106-118.

(2) Jeong, S., Murayama, M., and Yamamoto, K., Efficient Optimization Design Method Using Kriging Model, *Journal of Aircraft*, Vol. 42, No.2 (2005), pp.413-420.

(3) Koehler, J and Owen, A. Computer experiments, in S. Ghosh and C. R. Rao (eds.), Handbook of Statistics, 13: *Design and Analysis of Experiments*, *Elsevier, Amsterdam*(1996),pp. 261-308.

(4) Fonseca,C. M., and Fleming, P. J., Genetic Algorithms for Multiobjective Optimization: Formulation, Discussion and Generalization, *Proceedings of the 5th International Conference on Genetic Algorithms*(1993), pp. 416-423.

(5) Obayashi, S., Jeong, S., Chiba, K., and Morino, H., Multi-Objective Design Exploration and Its Application to Regional-Jet Wing Design, *Transaction of Japan Society for Aeronautical and Space Sciences*, Vol. 50, No. 167 (2007), pp. 1-8.

(6) Kohonen T., *Self-Organizing Maps*, (2000), Springer.

(7) Pawlak, Z., Rough Sets, *International Journal of Computer and Information Sciences*, Vol. 11, No. 5 (1982), pp. 341-356.

(8) Kanazaki, M., and Jeong, S., High-lift Airfoil Design Using Kriging based MOGA and Data Mining, *Korea Society for Aeronautical and Space Sciences International Journal*, Vol. 8, No. 2 (2007), pp. 28-36.

(9) Horinouchi, S., Conceptual Design of a Low Boom SSBJ, AIAA-2005-1018, (2005).

(10) Makino, Y., Low sonic-boom design of a Silent Super Sonic Technology Demonstrator ~ Development of CAPAS and its Application ~, *JAXA Special Publication, Proceedings of International Workshops on Numerical Simulation Technology for Design of Next Generation Supersonic Civil Transport* (2007), pp. 697-704.

(11) Chiba, K., Makino, Y., and Takatoya, T., Design-Informatics Approach for Intimate Configuration of Silent Supersonic Technology Demonstrator, AIAA-2009-968, (2009).
(12) Sack, J., Welch, W. J., Mitchell, T. J., and Wynn, H. P., Design and analysis of computer experiments (with discussion), *Statistical Science 4*, (1989), pp. 409-435.
(13) Owen, A. B., Orthogonal arrays for computer experiments, integration and visualization, *Statistica Sinica*, Vol. 2 (1992), pp. 439-452.
(14) Donald, R. J., Matthias S and William J. W, Efficient Global Optimization of Expensive Black-Box Function, *Journal of global optimization*, Vol. 13 (1998), pp. 455-492.
(15) Hiroyasu, T., Miki, M., and Watanabe, S., The New Model of Parallel Genetic Algorithm in Multi-Objective Optimization Problems (Divided Range Multi-Objective Genetic Algorithm), *IEEE Proceedings of the Congress on Evolutionary Computation 2000*, Vol.1 (2000), pp. 333-340.
(16) Mac Queen, J. B., Some Methods for classification and Analysis of Multivariate Observations, *Proceedings of 5-th Berkeley Symposium on Mathematical Statistics and Probability*, Berkeley, (1967), pp. 281-297.
(17) Vesant, J., SOM Based Data Visualization Method, *Intelligent-Data-Analysis*, Vol. 3 (1999), pp. 111-26.
(18) Raymer, P. D., *Aircraft Design: A Conceptual Approach*, *Fourth edition*, (2006).
(19) Darden, C. M., Sonic-Boom Minimization With Nose-Bluntness Relaxation, *NASA Technical Paper* 1348, (1979).